(Received 17 June 2026, Accepted 13 August 2026, Scheduled 5 September 2026)

Rectifier with Harmonic Communication for SWIPT Receiver Front-End of QFSK Modulation

Zhoulin Fan, Junfei Ji, Abubaker A. Elobied, Fan Yu, and Xue-Xia Yang*

School of Communication and Information Engineering, Shanghai University, Shanghai, China

ABSTRACT: This paper proposes a compact harmonic communication rectifier for a simultaneous wireless information and power transfer (SWIPT) receiver front-end employing quadrature frequency-shift keying (QFSK) modulation. First, we theoretically analyzed the feasibility of communication using the second harmonic of QFSK signals. Second, a compact harmonic communication rectifier is proposed by combining a frequency-selective duplexer and an impedance-matching network. The duplexer with two output branches partially extracts the low-power second harmonic for communication and fully transmits the fundamental wave for wireless power transfer. The matching network with π-type can transmit the fundamental wave to the diode for rectification and adjust the energy-information power ratio for practical requirements. Finally, the proposed rectifier is fabricated and measured with good agreement between simulation and measurement results. A rectifying efficiency of 76.7% is achieved for QFSK-modulated waves with a carrier frequency of 2.5 GHz and a frequency offset of 20 MHz at an input power of 14 dBm. The extracted second-harmonic power is -5.3 dBm with an energy-to-information power ratio of $64 : 1$. The signal-to-noise ratio (SNR) is 30 dB and the bit error rate (BER) is less than 10^{-12}.

1. INTRODUCTION

The development of sixth generation (6G) communication technologies is accelerating the evolution of the Internet of Things (IoT). The International Telecommunication Union (ITU) predicted in its white paper Framework for 2030 and beyond that the number of connected devices worldwide will exceed one trillion by 2030, with low-power IoT terminals accounting for more than 60% of these devices [1]. Most of these terminal devices are powered by batteries. However, batteries' limited capacity not only increases replacement and maintenance costs but also shortens the service life of devices and contributes to electronic waste. Simultaneous wireless information and power transfer (SWIPT) technology uses electromagnetic waves for both information transmission and energy harvesting through RF-to-DC power conversion [2]. Owing to high sensitivity of communication receivers, the power level required for energy harvesting is significantly higher than that required for information transmission. A signal power of -60 dBm can be sufficient for communication, whereas wireless energy transfer requires input power of at least -10 dBm to maintain a rectifying efficiency above 50% [3]. Moreover, the higher electromagnetic power required for energy harvesting is consistent with the power requirements of practical applications [4].

A rectifier is a key component at the receiving end of a SWIPT system and converts radio frequency (RF) power into direct-current (DC) power. Power dividers and couplers are commonly employed to split the fundamental RF signal carrying information into two paths. One path is directed to the rectifier for RF-to-DC power conversion, while the other is used for information reception [5–7]. Using these methods, energy-harvesting-to-information power ratios of $4 : 1$ [5], $3 : 3 : 4$ [6], and $1 : 1$ [7] have been achieved. In [8], an unequal power-dividing network is designed to achieve an approximate energy-to-information power ratio of $3 : 1$. However, these power-division methods are constrained by the realizable microstrip-line width, making it difficult to achieve large power-division ratios.

The nonlinear behavior of diodes generates harmonics during rectification. Using these harmonics for information transmission while using the fundamental-frequency signal for wireless power transfer eliminates the need for a dedicated power-division network. Since harmonic power is significantly lower than fundamental-frequency power, this approach naturally accommodates the large difference in power requirements between high-sensitivity communication receivers and RF energy-harvesting circuits. Harmonic extraction can be achieved by incorporating a dedicated harmonic-extraction circuit or by employing the harmonic source-pull technique. Rectifying efficiencies of 58% [9] and 71% [10], with corresponding second-harmonic output powers of -11 dBm [9] and -1 dBm [10], respectively, have been reported. In [11], the harmonic source-pull technique is employed to achieve impedance matching at both the fundamental and harmonic frequencies, eliminating the need for additional filters. A second harmonic output power of 0.17 dBm and a rectifying efficiency of 60.6% are achieved. In [12, 13], lower-power third harmonics are extracted through couplers to enhance the RF-to-DC conversion efficiency. However, these approaches are based on continuous-wave (CW) excitation and can provide only limited functions, such as positioning and tracking, by exploiting harmonics amplitude or phase information.

* Corresponding author: Xue-Xia Yang (yang.xx@shu.edu.cn).

doi:10.2528/PIERL26061702

In [14], an additional modulation circuit is introduced in which a variable capacitor is used to adjust the impedance and thereby amplitude-modulate the second harmonic, enabling transmission of baseband information at a data rate of 2 Mb/s.

Quadrature frequency-shift keying (QFSK) transmits digital information using four distinct frequencies, with each frequency representing a 2-bit symbol. QFSK features low power consumption and strong interference immunity, making it suitable for Internet of Things (IoT) applications such as wireless sensor nodes. In this work, the feasibility of QFSK-based harmonic communication is first theoretically analyzed. A compact harmonic communication rectifier combining a frequency-selective duplexer and an impedance-matching network is then proposed for the SWIPT receiver front end. The power level of the second harmonic for communication can be adjusted according to practical requirement. Finally, a prototype is fabricated and measured to validate its rectification and communication performances.

2. THEORETICAL ANALYSIS OF SECOND HARMONIC COMMUNICATION WITH QFSK MODULATION

The feasibility of information transmission using the second harmonic of the QFSK signal is theoretically analyzed. The time-domain expression of the QFSK signal is given by:

$$V_{in} = V\cos(\omega_n t) \quad n = 1, 2, 3, 4 \tag{1}$$

where ω_n denotes four distinct carrier angular frequencies, representing the transmitted information bits 00, 01, 10, and 11, respectively, and V is the voltage amplitude of the QFSK signal.

During rectification, the Schottky diode operates under large-signal conditions, and its nonlinear characteristics generate higher-order harmonics. The output signal V_o can be expressed as a Taylor-series expansion in terms of the input signal V_{in}:

$$V_o = k_0 + k_1 V_{in} + k_2 V_{in}^2 + k_3 V_{in}^3 + \ldots \tag{2}$$

where $k_0, k_1, k_2 \ldots$ are Taylor coefficients. Substituting Equation (1) into Equation (2) yields:

$$\begin{aligned} V_o &= k_0 + k_1[V\cos(\omega_n t)] + k_2[V\cos(\omega_n t)]^2 \\ &\quad + k_3[V\cos(\omega_n t)]^3 + k_4[V\cos(\omega_n t)]^4 + \ldots \end{aligned} \tag{3}$$

As shown in Equation (3), the second-harmonic component arises only from even-order terms in the Taylor-series expansion. The contributions to the second harmonic from the fourth- and higher-order even terms are relatively small compared with that from the second-order term and can therefore be neglected. By applying trigonometric identities, the second-order term in Equation (3) can be expanded as follows:

$$k_2[V\cos(\omega_n t)]^2 = k_2 V^2 \frac{1+\cos(2\omega_n t)}{2} \tag{4}$$

The time-domain expression of the second-harmonic component is given by:

$$V_{2\omega} = k_2 \frac{V^2}{2}\cos(2\omega_n t) \tag{5}$$

Compared with Equation (1), the amplitude of the second-harmonic component $V_{2\omega}$ is $k_2 V/2$ times that of the fundamental-frequency component, while its frequency is doubled. Both the carrier frequency and frequency offset of the second harmonic are twice those of the fundamental signal. Therefore, the second harmonic preserves the same baseband information as the fundamental signal and can consequently be utilized for information transmission.

3. STRUCTURE AND PERFORMANCE OF THE RECTIFIER WITH HARMONIC COMMUNICATION

Figure 1(a) shows the schematic of the proposed harmonic communication rectifier, which consists of a frequency-selective duplexer, an impedance-matching network, a Schottky diode, and a DC-pass filter. The incident RF signal is applied to Port 1, while the rectified DC power is delivered through Port 3. A dedicated impedance-matching network is designed to efficiently transmit the fundamental wave to the Schottky diode for rectification. A portion of the second-harmonic power generated by the diode during rectification propagates back toward the frequency-selective duplexer. The duplexer separates the second-harmonic component from the fundamental-frequency signal and routes it to Port 2 for information reception. The remaining harmonic power is prevented from propagating through the duplexer and is confined around the diode's input and output terminals, where it contributes to further rectification, reducing harmonic power loss.

Figure 1(b) shows the structure of the proposed rectifier. The circuit is fabricated on an F4B dielectric substrate with a relative permittivity of $\varepsilon_r = 2.65$, a loss tangent of $\tan\delta = 0.0013$, and a thickness of 0.8 mm. The rectifier is designed at the center frequency of 2.5 GHz with the total size of 59.72 mm × 43.56 mm ($0.5\lambda_0 \times 0.36\lambda_0$). Each component of the proposed rectifier is analyzed and simulated using Advanced Design System (ADS) software.

The frequency-selective duplexer consists of 50 Ω microstrip lines, a $\lambda/4$ microstrip line, and sector stubs. The $\lambda/4$ microstrip line and sector stubs serve as filters in the two branches, blocking signals at different frequencies. Consequently, separate transmission paths are provided for the fundamental wave and the second harmonic component, enabling extraction of the second harmonic. The specially designed duplexer ensures that the fundamental wave (f) is transmitted from Port 1 to Port 4 and subsequently delivered to the rectifier. Meanwhile, the second-harmonic component ($2f$) reflected by the DC-pass filter propagates back to Port 4 and is subsequently routed to Port 2 via the frequency-selective duplexer. T_3 is a $\lambda/4$ microstrip line designed to operate at the second-harmonic frequency, $2f_0$. According to transmission line theory, the input impedance of a lossless transmission line with characteristic impedance Z, electrical length θ, and load impedance Z_L is given by [15]

$$Z_{in} = Z_0 \frac{Z_L + jZ_0\tan\theta}{Z_0 + jZ_L\tan\theta} \tag{6}$$

When the electrical length $\theta = 90°$, i.e., physical length $= \lambda/4$, the input impedance becomes $Z_{in} = Z^2/Z_L$. With its terminal

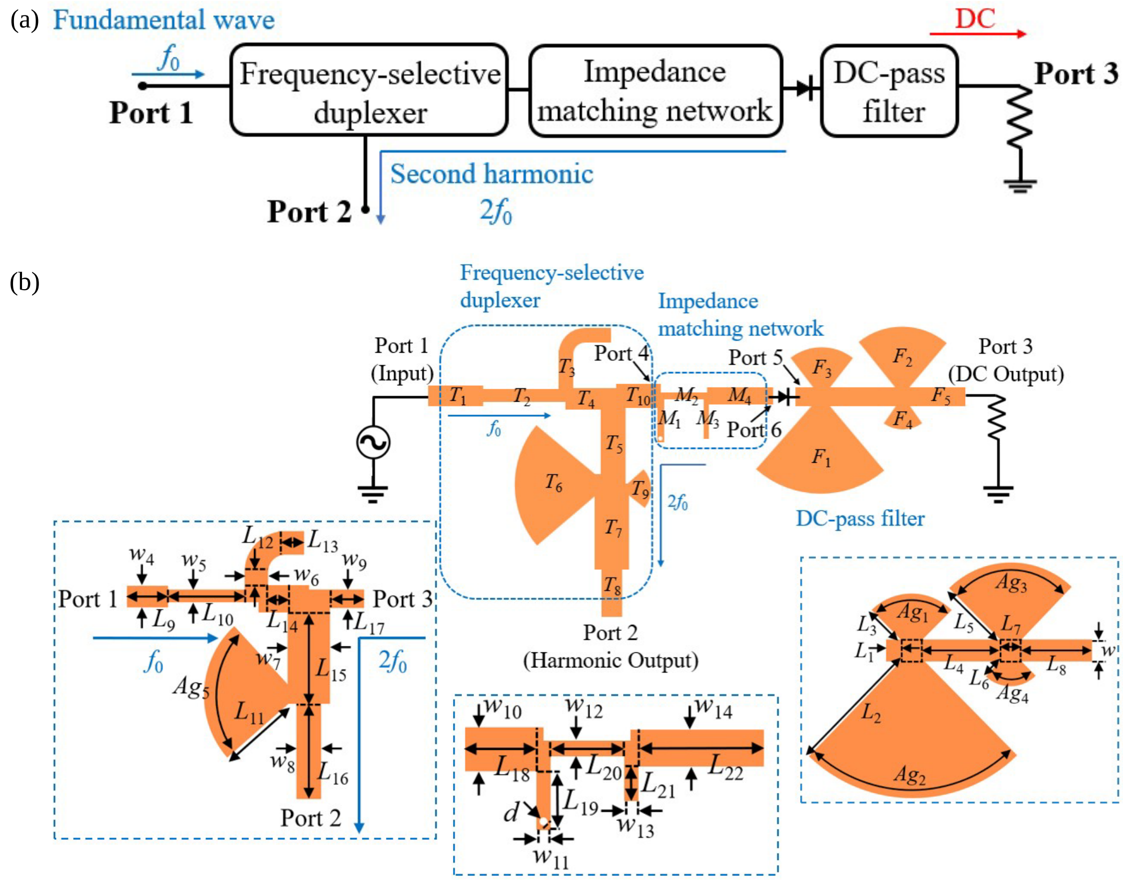

FIGURE 1. (a) Schematic diagram and (b) structure of harmonic communication rectifier ($L1 = 0.5\,\text{mm}$, $L2 = 12.86\,\text{mm}$, $L3 = 5.03\,\text{mm}$, $L4 = 7\,\text{mm}$, $L5 = 7\,\text{mm}$, $L6 = 2.8\,\text{mm}$, $L7 = 1.5\,\text{mm}$, $L8 = 7\,\text{mm}$, $Ag1 = 70°$, $Ag2 = 80°$, $Ag3 = 70°$, $Ag4 = 70°$, $w = 1.5\,\text{mm}$, $L9 = 4\,\text{mm}$, $L10 = 9.92\,\text{mm}$, $L11 = 10\,\text{mm}$, $L12 = 3\,\text{mm}$, $L13 = 2.98\,\text{mm}$, $L14 = 1\,\text{mm}$, $L15 = 10.84\,\text{mm}$, $L16 = 14\,\text{mm}$, $L17 = 2\,\text{mm}$, $w4 = 2.11\,\text{mm}$, $w5 = 1\,\text{mm}$, $w6 = 2.63\,\text{mm}$, $w7 = 4.4\,\text{mm}$, $w8 = 2.11\,\text{mm}$, $w9 = 2.11\,\text{mm}$, $Ag5 = 100°$).

open-circuited ($Z_L \to \infty$) the input impedance at $2f$ becomes $Z_{in} \to 0$. The physical length of T_3 is determined by

$$L_{T3} = \frac{\lambda_g}{4} = \frac{c}{4 \times 2f_0 \times \sqrt{\varepsilon_{eff}}} \tag{7}$$

It is designed to suppress transmission of the second-harmonic component from Port 4 to Port 1, while its bent configuration is used to reduce the overall circuit size. The sector stub T_6 prevents the fundamental wave from leaking into the second-harmonic output path. Another sector stub T_9 is designed to further suppress the third-harmonic component, reducing its potential interference with second-harmonic demodulation. The initial radii and angular dimensions of the microstrip sector stubs T_6 and T_9 are calculated using the closed-form expressions derived in [16], and their final dimensions are optimized via ADS simulations. Resulting design parameters are as follows: T_3 has a width of 1.0 mm and a length of 10.3 mm; T_6 has a radius of 14.8 mm and an angle of 70°; and T_9 has a radius of 4.0 mm and an angle of 70°.

Figure 2(a) shows simulated S-parameters of the frequency-selective duplexer. At f_0, $|S_{41}| = -0.02\,\text{dB}$, and $|S_{21}| < -20\,\text{dB}$, indicating that the fundamental-frequency signal is efficiently transmitted from Port 1 to Port 4 while being effectively suppressed from Port 1 to Port 2. At $2f_0$, $|S_{24}| = -0.03\,\text{dB}$ and $|S_{14}| < -20\,\text{dB}$, demonstrating that the second-harmonic signal is efficiently transmitted from Port 4 to Port 2 while being effectively suppressed from Port 4 to Port 1. At $3f_0$, $|S_{24}| < -20\,\text{dB}$, indicating that the third-harmonic signal is effectively suppressed along the path from Port 4 to Port 2 and confirming the third-harmonic suppression provided by the sector stub T_9.

The DC-pass filter consists of four sector stubs (F_1, F_2, F_3, F_4), which are designed to reflect the fundamental, second, third, and fourth harmonic components, respectively, while allowing the DC component to pass. The design procedure for each stub is similar to that used for T_6 and T_9. The radius of each sector stub determines its filtering frequency, and the sector angle affects the filtering effect. After optimization, the radii of F_1, F_2, F_3, and F_4 are 12.9, 7.0, 5.0, and 2.8 mm, respectively. The angle of F_1 is 80°, and those of F_2, F_3, and F_4 are 70°. Figure 2(b) shows simulated S-parameters of the DC-pass filter. At the harmonic frequencies, $|S_{35}| < -20\,\text{dB}$ and $|S_{55}|$ dB is close to 0 dB, indicating effective harmonic suppression and reflection. The frequency-selective duplexer exhibits a -10-dB bandwidth of approximately 610 MHz, while the DC-pass filter provides a bandwidth of approximately 6.6 GHz.

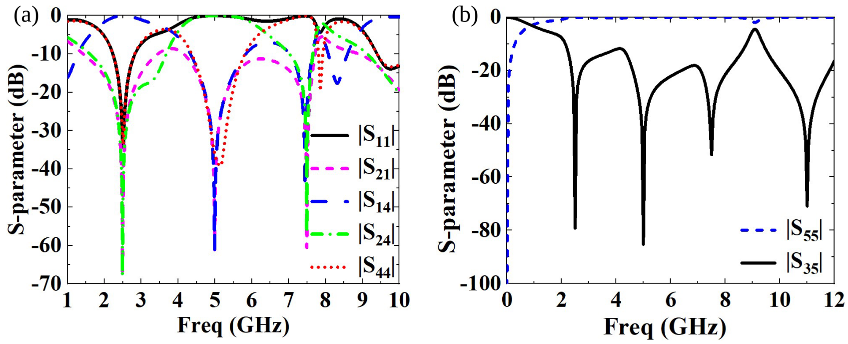

FIGURE 2. Simulated S-parameter results of (a) frequency-selective duplexer and (b) DC-pass filter.

HSMS2860 Schottky diode is selected as the rectifying diode. The maximum harmonic order is set to the 5th order because even higher-order harmonics are very low. The impedance matching network between the output of the frequency-selective duplexer (Port 4) and the input of the rectifying diode (Port 6) serves two functions. First, it transforms the diode's complex input impedance to $50\,\Omega$ at f_0, achieving impedance matching for efficient power transfer from the source to the rectifier. Second, it allows a portion of the second-harmonic power ($2f_0$) generated by the diode to propagate back toward the duplexer with low loss and subsequently be routed to Port 2 for information transmission. Due to nonlinear characteristics of the Schottky diode, its input impedance varies with input power level and load resistance. At 2.53 GHz, with an input power of 14 dBm and a load resistance of $400\,\Omega$, the diode input impedance is (3.132-j325) Ω, indicating a strongly capacitive input impedance. Accordingly, a π-type impedance matching network is designed to transform this complex impedance to $50\,\Omega$. M_1, M_2, and M_4 are employed to achieve impedance matching at the fundamental frequency f_0. As a short-circuited shunt transmission line with an electrical length of less than $\lambda/4$, M_1 exhibits inductive reactance and is therefore used to compensate for the diode's capacitive reactance. The open-circuited stub M_3 is used to control the transmission coefficient $|S_{46}(2f_0)|$ between the diode and the duplexer (Port 4). A portion of the second-harmonic power is transmitted toward Port 4 and subsequently routed to Port 2, while the remaining portion is reflected toward the diode and contributes to further rectification. Therefore, M_3 controls the second-harmonic output power at Port 2. Figure 3 shows the variation in the second-harmonic output power at Port 2 as a function of the length of stub M_3. Considering the trade-off between energy-harvesting efficiency and communication performance, length M_3 is selected as 4.75 mm.

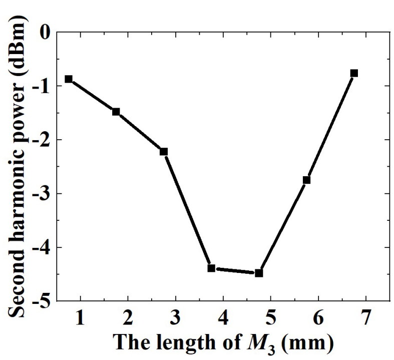

FIGURE 3. Second harmonic power at Port 2 versus lengths of M_3.

Figure 4 shows the simulated reflection coefficient, rectifying efficiency, and second-harmonic output power of the proposed rectifier as functions of frequency, when the circuit is excited by a 14 dBm continuous wave (CW) signal with a load resistance of $400\,\Omega$. At 2.53 GHz, $|S_{11}| = -24$ dB, the rectifying efficiency reaches 83%, and the second harmonic output power at Port 2 is -4.5 dBm. In addition, the rectifying efficiency remains relatively stable around the center frequency, indicating that the rectifier can maintain consistent energy-harvesting performance over the operating frequency range. Therefore, the rectifying efficiency under QFSK-modulated excitation is expected to be close to that obtained under CW excitation. When a QFSK-modulated signal with a carrier frequency of $f_c = 2.53$ GHz and a frequency offset of $\Delta f = 20$ MHz is applied to the rectifier, a rectifying efficiency of 80% is achieved, with the second-harmonic output power of -4 dBm at Port 2.

4. EXPERIMENTAL VERIFICATION

The proposed harmonic communication rectifier is fabricated and experimentally characterized. The rectifier's reflection coefficient is measured using a vector network analyzer (VNA). Figure 5 shows the experimental setup used to evaluate rectifying efficiency and communication performance. The transmitting system consists of a signal generator, a power amplifier, and a directional coupler. The coupled port of the directional coupler is connected to a power sensor to monitor the input power P_{in} using a power meter, while the through port is connected to the rectifier's input port. A voltmeter is used to measure the rectified DC output voltage V_{out}. The rectifying efficiency η is calculated using Equation (8):

$$\eta = \frac{P_{out}}{P_{in}} = \frac{V_{out}^2}{R_L \cdot P_{in}} \tag{8}$$

First, the rectifying performance under CW excitation is experimentally evaluated. The signal generator produces a CW signal, while the rectifier's harmonic output port (Port 2) is terminated with a matched load. Figure 6(a) shows the measured $|S_{11}|$ and rectifying efficiency responses as functions of frequency at a CW input power of 14 dBm and a load resistance

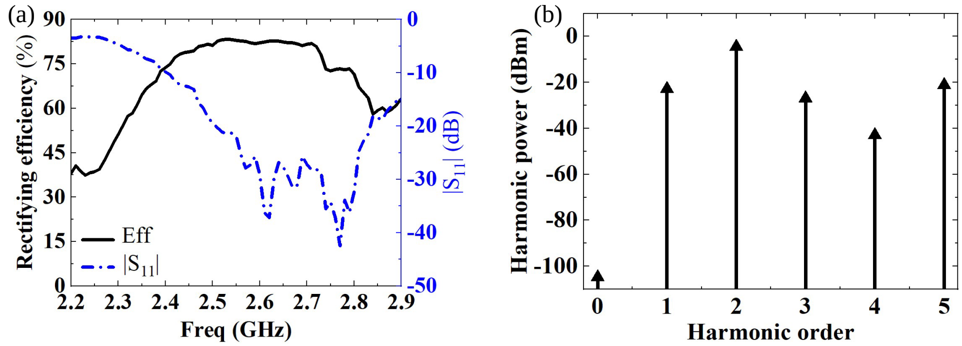

FIGURE 4. Simulated results of the harmonic communication rectifier. (a) Rectifying efficiency and $|S_{11}|$ frequency response curves of CW and (b) harmonic power of each order at Port 2.

TABLE 1. Comparison of rectifiers for SWIPT receiver front-ends.

References	Power division implementation method	Frequency (GHz)	Input power (dBm)	Rectifying efficiency	Signal type	*Energy-to-information power ratio
[5]	Asymmetrical coupler	2.4	6	70.4%	QPSK	4 : 1
[6]	Ring coupler	5	10	74.2%	CW	1 : 1 : 1
[7]	Reverse Wilkinson power divider	2.45/5.8	10	75.3%	CW	1 : 1
[9]	Second harmonic	0.915/1.83	5	58%	CW	32 : 1
[10]	Second harmonic	0.915/1.83	15	71%	CW	41 : 1
[17]	Second harmonic	2.6	3	55.2	CW	5.27 : 1
[18]	Second harmonic	2.6	3	47	CW	3.46 : 1
This work	Second harmonic	2.5/5	14	76.7%	QFSK	64 : 1

*The energy-to-information power ratios presented refer to those of the experimental samples; the power ratios in [9] and [10] were not provided in the original papers and were calculated by the presented data.

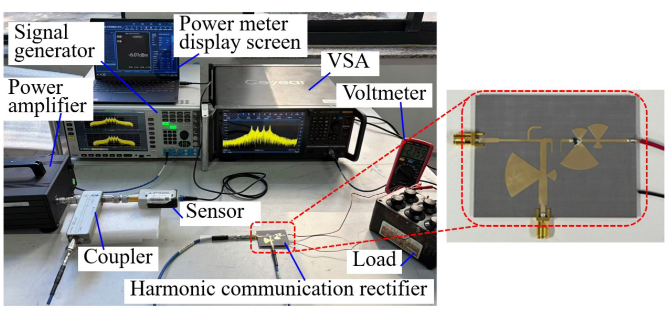

FIGURE 5. Measurement system of the communication rectifier.

of 400 Ω. The rectifying efficiency exceeds 70% over the frequency range from 2.34 to 2.64 GHz, and the second harmonic output power at Port 2 is -4.9 dBm.

The rectifier's communication performance is evaluated under QFSK-modulated excitation. As shown in Figure 5, the signal generator generates a QFSK-modulated signal, and the matched load is replaced by a vector signal analyzer (VSA) to observe the communication characteristics. The QFSK signal is centered at a 2.5 GHz carrier frequency and uses four frequencies, 2.47, 2.49, 2.51, and 2.53 GHz. The frequency spacing between adjacent frequency points is 20 MHz, which guarantees the orthogonality between different frequency symbols. The symbol rate of the QFSK signal is set to 5 Msymbol/s. Since each QFSK symbol carries 2-bit information, the corresponding bit rate is 10 Mbit/s. A raised-cosine filter with a roll-off factor of 0.5 is adopted for pulse shaping to suppress out-of-band spectral leakage and reduce inter-symbol interference.

Figure 6(b) shows the measured rectifying efficiency and DC output voltage as functions of the input power on a 400 Ω load when the QFSK-modulated signal is input. Throughout the 6–16 dBm test range, the output DC voltage rises monotonically with input power, while the rectification efficiency maintains a steady upward trend until it reaches its peak at 15 dBm input power. To guarantee long-term stable operation, 14 dBm is applied as the input power, at which the circuit achieves a DC output voltage V of 2.76 V and a rectification efficiency of 76.7%. The second-harmonic output power of -5.3 dBm is read at Port 2 at the same time. Considering the DC power of V/R_L, the energy-to-information power ratio is $64:1$.

To test communication characteristics, the original baseband sequence of the transmitted QFSK signal is preloaded into the VSA as the reference. The VSA demodulates the received second-harmonic QFSK signal, performs bit-by-bit comparison between the demodulated data and the preloaded reference sequence, and calculates the BER in real time. The continuous measurement duration is set to 100 s. With the adopted bit rate of 10 Mbit/s, the total number of bits under test reaches 10^9 over the full measurement period, which ensures sufficient statistical

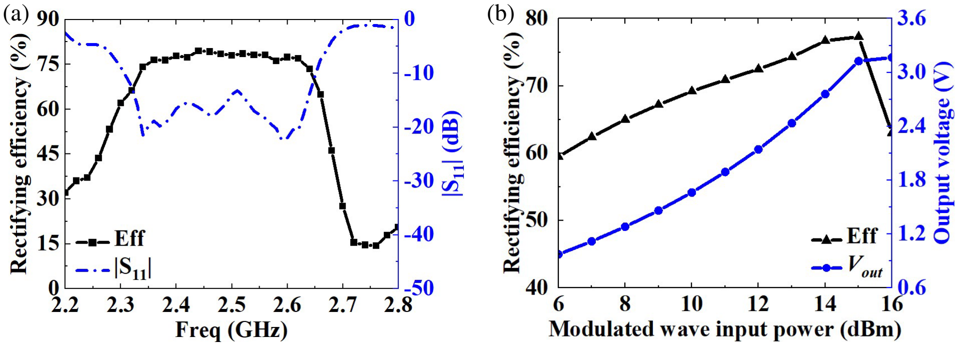

FIGURE 6. Measured results under (a) CW input and (b) QFSK-modulated wave input.

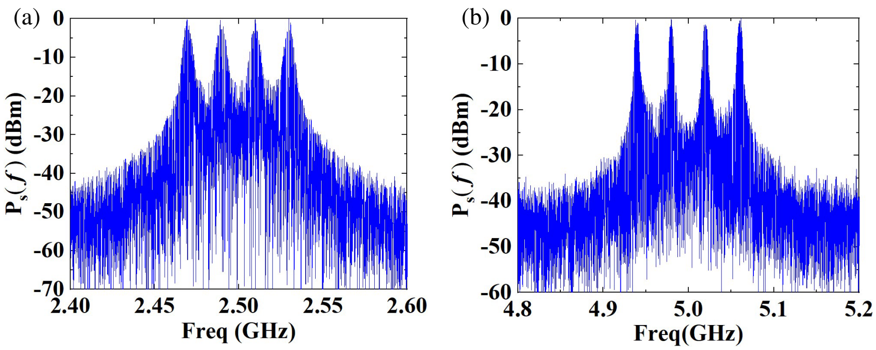

FIGURE 7. Comparison of input-output normalized spectrogram. (a) Input and (b) output.

confidence in the result. No bit error was detected in the entire measurement period. The BER reading on the VSA interface remained at 0, and the reading for signal-to-noise ratio (SNR) was 30 dB. Since the minimum measurable BER resolution of the VSA is 10^{-12}, the BER of this harmonic communication can be regarded as less than 10^{-12}.

Figure 7 shows the normalized spectra of the QFSK signal applied to the rectifier and the corresponding extracted second harmonic signal demodulated by the VSA. Both the carrier frequency and the frequency offset of the second-harmonic signal are twice those of the input QFSK signal, consistent with the theoretical derivation.

Table 1 compares the performance of the proposed rectifier with that of recently reported rectifiers for SWIPT receiver front-ends. Except for the proposed design and Ref. [5], all designs are about CW. By employing harmonic communication, the proposed design achieves a high efficiency of 76.7%, a large energy-to-information power ratio of $64 : 1$. Its power ratio and rectifying efficiency are comparable to those reported in [10]. However, the design in [10] employs lumped elements, which may limit its applicability at higher operating frequencies due to the parasitic effects of these components.

5. CONCLUSION

In this paper, a compact harmonic communication rectifier for the SWIPT receiver front-end of QFSK modulation is proposed. It converts electromagnetic energy into DC power to supply low-power terminal devices and simultaneously enables communication via the generated second harmonic. Experimental results demonstrate that for QFSK signals with a carrier frequency $f_c = 2.5$ GHz and a frequency offset $\Delta f = 20$ MHz, the rectifier achieves a rectifying efficiency of 76.7%. The signal power at the second harmonic output port is -5.3 dBm, and the communication bit error rate (BER) is less than 10^{-12}. The second-harmonic power can be adjusted at the design stage according to practical requirement. The proposed rectifier realizes rational energy utilization and provides a novel solution for IoT's large-scale deployment. It should be pointed out that the proposed design can be extended to higher-order modulation of nFSK ($n = 8, 16 \ldots$) only if frequencies are within the operating band of high rectifying efficiency.

ACKNOWLEDGEMENT

This work was supported by the National Natural Science Foundations of China under Grant 62171270.

REFERENCES

[1] ITU, "WP5D I. Draft new recommendation ITU-R M. [IMT. Framework for 2030 and beyond]," 2023.

[2] Varshney, L. R., "Transporting information and energy simultaneously," in *2008 IEEE International Symposium on Information Theory*, 1612–1616, Toronto, ON, Canada, Jul. 2008.

[3] Bi, S., Y. Zeng, and R. Zhang, "Wireless powered communication networks: An overview," *IEEE Wireless Communications*, Vol. 23, No. 2, 10–18, Apr. 2016.

[4] Nafiaa, R. E. and A. Z. Yonis, "Analysis of frequency splitting phenomenon in WPT for intelligent applications," in *2022 IEEE International Conference on Automatic Control and Intelligent Systems (I2CACIS)*, 174–179, Shah Alam, Malaysia, 2022.

[5] Lu, P., K. Huang, C. Song, Y. Ding, and G. Goussetis, "Optimal power splitting of wireless information and power transmission using a novel dual-channel rectenna," *IEEE Transactions on Antennas and Propagation*, Vol. 70, No. 3, 1846–1856, Mar. 2022.

[6] Cao, C., X. Zhang, C. Song, A. Georgiadis, and G. Goussetis, "A highly integrated multipolarization wideband rectenna for simultaneous wireless information and power transfer (SWIPT)," *IEEE Transactions on Antennas and Propagation*, Vol. 71, No. 10, 7980–7991, Oct. 2023.

[7] Zhang, X., C. Cao, and C. Song, "A compact dual-band dual-circular-polarization wideband rectenna using reverse wilkinson power divider for wireless information and power transfer," *IEEE Antennas and Wireless Propagation Letters*, Vol. 23, No. 9, 2728–2732, Sep. 2024.

[8] Zhu, G.-L., J.-X. Du, X.-X. Yang, Y.-G. Zhou, and S. Gao, "Dual-polarized communication rectenna array for simultaneous wireless information and power transmission," *IEEE Access*, Vol. 7, 141 978–141 986, 2019.

[9] Shen, J., W. Zhang, C. Wu, X. Wu, E. Fang, and X. Liu, "A compact duplexing rectenna with wireless power transfer and harmonic feedback capabilities," *IEEE Antennas and Wireless Propagation Letters*, Vol. 22, No. 7, 1751–1755, Jul. 2023.

[10] Joseph, S. D., Y. Huang, S. S. H. Hsu, A. Alieldin, and C. Song, "Second harmonic exploitation for high-efficiency wireless power transfer using duplexing rectenna," *IEEE Transactions on Microwave Theory and Techniques*, Vol. 69, No. 1, 482–494, Jan. 2021.

[11] Kawai, K., N. Shinohara, and T. Mitani, "Design of a second harmonic reradiating rectenna using harmonic source pull," *IEEE Transactions on Microwave Theory and Techniques*, Vol. 72, No. 10, 6164–6173, Oct. 2024.

[12] Zhang, H., Y.-X. Guo, S.-P. Gao, and W. Wu, "Wireless power transfer antenna alignment using third harmonic," *IEEE Microwave and Wireless Components Letters*, Vol. 28, No. 6, 536–538, Jun. 2018.

[13] Zhang, H., Y.-X. Guo, S.-P. Gao, Z. Zhong, and W. Wu, "Exploiting third harmonic of differential charge pump for wireless power transfer antenna alignment," *IEEE Microwave and Wireless Components Letters*, Vol. 29, No. 1, 71–73, Jan. 2019.

[14] Wu, P., S.-P. Gao, Y.-D. Chen, Z. H. Ren, P. Yu, and Y. Guo, "Harmonic-based integrated rectifier-transmitter for uncompromised harvesting and low-power uplink," *IEEE Transactions on Microwave Theory and Techniques*, Vol. 71, No. 2, 870–880, Feb. 2023.

[15] Pozar, D. M., *Microwave Engineering*, 4th ed., John Wiley & Sons, 2012.

[16] Sorrentino, R. and L. Roselli, "A new simple and accurate formula for microstrip radial stub," *IEEE Microwave and Guided Wave Letters*, Vol. 2, No. 12, 480–482, Dec. 1992.

[17] Zhang, C., Y. Wang, Z. Zhu, S. Sun, J. Shi, Y. He, P. Lu, and C. Song, "Rectenna-enabled new paradigm with hybrid harmonic beamforming for integrated energy harvesting, sensing, and communications," *IEEE Transactions on Antennas and Propagation*, Vol. 73, No. 1, 121–134, Jan. 2025.

[18] Zhu, Z., Y. Wang, Q. Liao, Y. Ke, S. Sun, C. Zhang, and C. Song, "Design of a duplex rectifier with high-efficiency second harmonic generation," *IEEE Microwave and Wireless Technology Letters*, Vol. 35, No. 10, 1530–1533, Oct. 2025.